Graphene Paper Doped with Chemically Compatible Prussian Blue Nanoparticles as Nanohybrid Electrocatalyst

*Nan Zhu, Shuang Han, Shiyu Gan, Jens Ulstrup, and Qijin Chi**

Along with reduced graphene oxide (RGO), water soluble Prussian blue nanoparticles (PBNPs, around 6 nm) are synthesized and broadly characterized. These two types of highly stable, low-cost and chemically compatible nanomaterials are exploited as building ingredients to prepare electrically enhanced and functionally endorsed nanohybrid electrocatalysts, which are further transformed into free-standing graphene papers. PBNPs doped graphene papers show highly efficient electrocatalysis towards reduction of hydrogen peroxide and can be used alone as flexible chemical sensors for potential applications in detection of hydrogen peroxide or/and other organic peroxides. The as-prepared PBNPs–RGO papers are further capable of biocompatible accommodation of enzymes for development of free-standing enzyme based biosensors. In this regard, glucose oxidase is used as an example for electrocatalytic oxidation and detection of glucose. The present work demonstrates a facile and highly reproducible way to construct free-standing and flexible graphene paper doped with electroactive catalyst. Thanks to high stability, low-cost and efficient electrocatalytic characteristics, this kind of nanohybrid material has potential to be produced on a large scale, and offers a broad range of possible applications, particularly in the fabrication of flexible sensing devices and as a platform for electrocatalytic energy conversion.

1. Introduction

Graphene papers are a novel type of layered materials emerged very recently. Since the pioneering work reported by Ruoff and co-workers in 2007,[1] graphene paper has added an attractive form to the scientific catalogue of rapidly surging graphene-based nanomaterials. Through wet-chemical methods,[2,3] graphene papers can be made of either graphene oxide (GO) or reduced graphene oxide (RGO) by relatively simple and low-cost procedures that involve synthesis and vacuum filtration of individual and liquid suspended graphene nanosheets.[1] As a free-standing material, graphene paper has several remarkable characters, reflected by practically high electrical conductivity, mechanical robustness, excellent thermal stability, structural uniformity, and geometric flexibility.[1] These features have altogether enabled expanding the application scope of graphene materials to a much wider range of various demands. Several possible applications have been demonstrated mainly at the laboratory level, for example, the use for flexible sensors,[4–9] energy storage,[10–18] biocompatible materials,[19–21] and even antibacterial agents.[22,23] With still limited exploration to date, however, the development of graphene papers and their applications in various areas remain at the infant stage. In the other words, there is plenty of room at the bottom to explore unfulfilled potentials of graphene papers as an advanced materials source. Three major research lines towards this end are anticipated and currently being carried out in parallel: 1) refinement and optimization of preparation procedures to further enhance electrical and mechanical properties,[24–28] 2) high-resolution structural characterization towards the atomic scale understanding of structural features and their relations to physicochemical properties,[29,30] and 3) versatile modifications of graphene papers to endorse specific and new functions.[31]

Functionalization is an essential step for most possible applications of graphene papers, because this material itself lacks desired specific functions such as catalysis, redox activity and molecular recognition. Decoration of graphene paper with nanoparticles (NPs) represents one of the most attractive ways for catalytic functionalization of this material that can be consistently used, for example, for sensing devices and energy conversion. This has been achieved by several different methods such as electrodeposition,[5,6] two-phase interfacial transfer,[7] and polymer-assisted encapsulation,[20] with most studies focused on metallic and metal oxide nanoparticles. Also, in these studies decoration (or modifications) is limited largely to the surface of graphene papers rather than inter-layered integration of functional materials into graphene papers. Recent efforts have offered an alternative approach.[8,31–33] For example, nanoparticles were first mixed with graphene nanosheets to prepare hybrid nanosheets, and this was then followed by flow-directed assembly of these individual hybrid nanosheets into graphene papers. A shortcoming of this approach is the lack of specific and robust interaction between the nanoparticles and graphene

N. Zhu, Dr. S. Han, S. Gan, Prof. J. Ulstrup, Prof. Q. Chi
Department of Chemistry
Technical University of Denmark
DK-2800 Kongens Lyngby, Denmark
E-mail: cq@kemi.dtu.dk

DOI: 10.1002/adfm.201300605

nanosheets. This could result in poor stability (e.g., leakage) and non-uniform distribution (e.g., aggregation) of nanoparticles in the graphene papers, as in most cases nanoparticles are only physically confined in the papers.

Materials that possess high stability, excellent electrocatalytic activity, low-cost and scaliabity of mass production are ideal electrocatalysts. Prussian blue (PB) and its analogues offer these merits and are arguably representatives of such idealized electrocatalysts.[34] PB thin films, often prepared by electrochemical methods, have been extensively used as electocatalyst in electrochemical sensors and biosensors.[35–39] A latest effort by Yao and co-workers, in which PB was synthesized directly into carbon nanotubes, shows new perspectives of this material as an attractive component in preparation of carbon-PB nanocomposites and their applications in biosensing devices.[40] However, there are three drawbacks generally associated with PB materials as electrocatalysts: 1) both PB powder and thin films prepared by either electrochemical or chemical methods are highly insoluble in water, 2) the conductivity is low, and 3) PB in neutral and alkaline solutions is unstable, although the material is extremely stable in its solid form. These shortcomings have limited one exploiting the full potential of this material. For example, due to insolubility, it is hardly possible to study the PB's electroactivity and/or to prepare biologically conjugated PB hybrid materials in homogeneous aqueous solutions. The low conductivity limits its application in electronic devices, and the lack of stability in neutral or alkaline media has excluded the coupling of PB with many oxidases that otherwise display their best catalytic activity at relatively high pH (>8).

In this work, we have demonstrated that: 1) water soluble and highly stable PB in the form of nanoparticles (PBNPs) can be synthesized; 2) PBNPs are chemically compatible with RGO nanosheets to form stable PBNPs–RGO nanohybrid sheets; 3) the resulting nanohybrid sheets can be stored either in solid form or solution dispersions with high stability; and 4) individual nanohybrid sheets can be transformed into free-standing graphene papers for electrocatalysis and construction of flexible sensors.

2. Results and Discussion

The overall procedure for preparation of PBNPs–RGO nanosheets and graphene papers, with emphasis on the crucial steps, is illustrated in **Scheme 1**. In the following five sections, we present the main experimental observations, accompanied by broad discussions. We start from the synthesis and characterization of PBNPs and nanohybrid PBNPs–RGO sheets. This is followed by description of preparation and critical properties of PBNPs doped graphene papers. The functional tests of the hybrid graphene papers as electrocatalysts in prototypes of electrochemical sensors and biosensors are presented in the final section.

2.1. Synthesis and Characterization of PBNPs

The synthesis of PBNPs was based on a recently reported method.[41] In order to obtain pure, water soluble and highly stable nanoparticle dispersions, the procedure was refined to include three essential steps.[42] Experimental details are given in the Supporting Information.

The synthesized nanoparticles (NPs) were well dispersed in pure water (or/and buffer solutions) and displayed high stability. For example, the first batch sample dispersed in pure water was prepared in 2008 and stored at room temperature. The PBNP dispersions were examined by UV-vis spectroscopy, transmission electron microscopy (TEM), atomic force microscopy (AFM) and electrochemistry. After more than three years, there was no detectable aggregation or changes in physicochemical properties (the final experimental examination was carried out in 2011, after three and half years). The stability of PBNPs prepared with the present method is, thus, among the best for all so far known or ever synthesized NPs.

We have gathered the information regarding basic optical property, morphology, size distribution and electroactivity (Supporting Information, Figures S1–S5), by systematic physical characterization using UV-vis spectroscopy, TEM, AFM and electrochemistry. Low concentration PBNPs solutions are transparent and exhibit blue color (**Figure 1**A; Supporting Information, Figure S1A). The absorption spectra are characterized mainly by a strong maximum absorbance around 700 nm (Supporting Information, Figure S1B). As a mixed-valence compound, PB absorbs orange-red light at 680 nm, so that the transmitted light appears blue, and this characteristic is retained for colloid PBNPs dispersions. In addition, the blue color is also associated with photo-induced electron transfer from Fe(II) to Fe(III). TEM and AFM images have shown that PBNPs are spherically shaped with an average size of 5.6 nm (Supporting

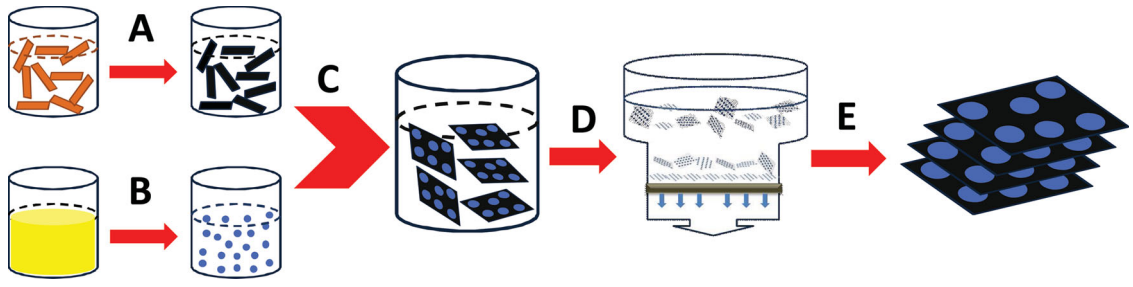

Scheme 1. Schematic illustration of the experimental procedures. A) Wet-chemical conversion of GO to RGO via hydrazine reduction, B) synthesis of PNBPs starting from the mixture of $FeCl_3$ and $K_4Fe(CN)_6$, C) preparation of PBNPs–RGO hybrid nanosheets, and D,E) processes of preparing PBNPs–RGO hybrid paper including filtration, drying and annealing. Not drawn to scale.

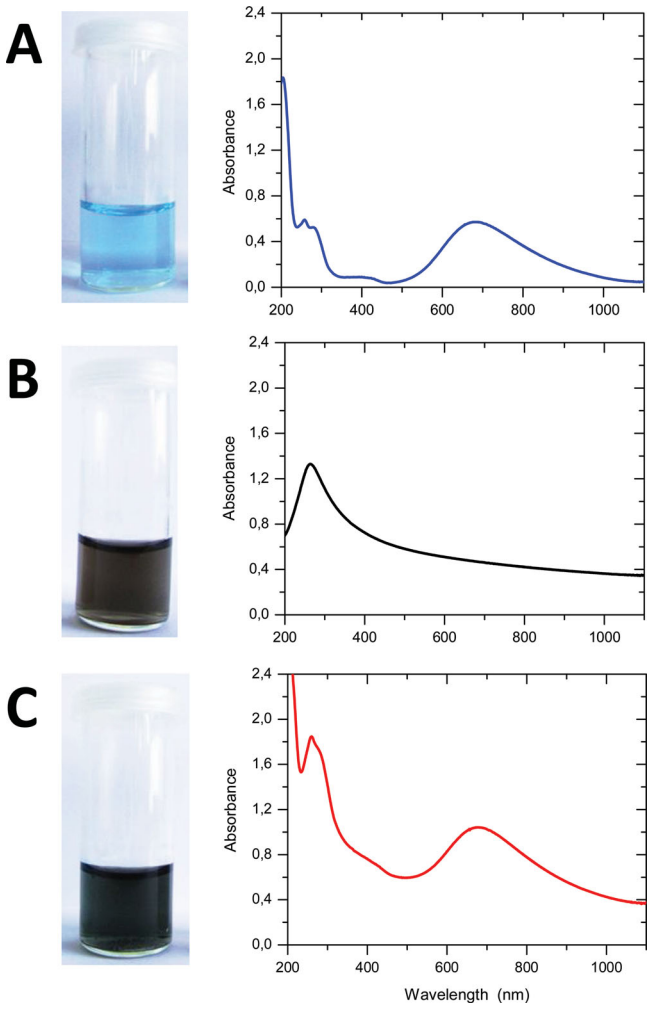

Figure 1. Sample photographs (left) and UV-vis spectra (right) of various colloid dispersions. A) PBNPs (blue curve), B) RGO (black curve), and C) PBNPs–RGO hybrid (red curve) solutions.

Information, Figures S2,S3). The size distribution is relatively narrow, even though the preparation of monodisperse PBNPs remains a challenge and is one of the major focuses in ongoing efforts. Furthermore, PBNPs are highly electroactive, as evidenced by electrochemical data. Well-defined cyclic voltammograms (CVs) with low background currents were obtained for PBNPs using single-crystal Au(111) as working electrodes. An example is given in Figure S4A (Supporting Information), in which the CVs with different scan rates are shown. The formal redox potential estimated from the midpoint of the anodic and cathodic peak potentials is around 0.15 V (vs. SCE), similar to that of PB films.[35,36] The linear dependence of both anodic and cathodic peak currents on the square root of scan rates indicate that the electrochemical reactions are diffusion-controlled (Supporting Information, Figure S4B). There is no detectable adsorption of the PBNPs on bare Au(111) surfaces. However, PBNPs can be well confined on Au(111) surfaces modified with thiol self-assembled monolayers (SAMs) via non-covalent interactions (Supporting Information, Figure S5). This observation is similar to previous reports where polymer-capping PBNPs and polycrystal gold electrodes were used.[43,44] Overall, these PBNPs retain the intrinsic electroactivity of PB materials and behave like large redox molecules such as metalloproteins, facilitating their redox properties to be studied and controlled by electrochemical approaches in detail.

2.2. Formation of PBNPs–RGO Hybrid Nanostructures

High-quality and stable GO was synthesized and characterized according to our recent report (experimental details also provided in the Supporting Information).[45] RGO was obtained by wet-chemical reduction of GO using hydrazine. As expected, chemical reduction of GO resulted in a solution color change from yellow to dark brown and the absorption red-shifted from 231 nm to 270 nm (Figure 1B). These observations support that the sp^2 electronic configuration in the graphene planes was largely restored upon chemical reduction. The lateral dimensions of synthesized RGO nanosheets vary from a few hundred nanometers to one micrometer, but their thickness (≈0.6 nm) is within expectations for single RGO layers as proven by AFM (Supporting Information, Figure S6).

To prepare PBNPs–RGO hybrids, PBNPs and RGO solutions were mixed under gentle stirring for at least two hours. This was followed by centrifugation for about 10 min. The sediment was then collected, while the supernatant was disregarded. The sediment was then re-dispersed uniformly in pure water. The PBNPs–RGO dispersion exhibits a dark green color and is characterized by two UV-vis absorption at 270 and 700 nm, respectively, which arise from each of the two building components (see, for example, Figure 1C). Compared to RGO solutions, PBNPs–RGO dispersions are significantly more stable. While the former lasts typically a few days before visible precipitation occurs by aggregation, the latter remains well dispersed for several months. This observation suggests that PBNPs stabilized the RGO nanosheets by preventing their hydrophobic and/or π–π stack interactions, attributed to the strongly hydrophilic and water stable features of PBNPs as described in Section 2.1. The chemical nature of the interaction between PBNPs and RGO nanosheets is not fully understood, but a major driving force is likely to be electrostatic attraction. This is suggested strongly by AFM and TEM imaging observations. AFM and TEM images show that PBNPs are adsorbed on the surfaces of RGO nanosheets with an overall uniform distribution (**Figure 2**; Supporting Information, Figure S7). High-resolution AFM images further reveal that PBNPs are predominantly located at the edges and wrinkles of RGO nanosheets (Figure 2B,C), where oxygen-containing functional groups are relatively abundant, and serve as linking groups for electrostatic attraction. This is consistent with the fact that PBNPs are stably immobilized on Au(111) surfaces modified with carboxylic groups terminated SAMs (Supporting Information, Figure S5).

In short, highly stable PBNPs–RGO hybrid nanosheets can be prepared by mixing two components. Intrinsic chemical interactions allow PBNPs to be confined on the surfaces of RGO nanosheets, predominantly adsorbed at edges and wrinkles. Electrostatic attraction appears to play a key role in the formation of PBNPs–RGO hybrids through oxygen-containing functional groups serving as linking groups.

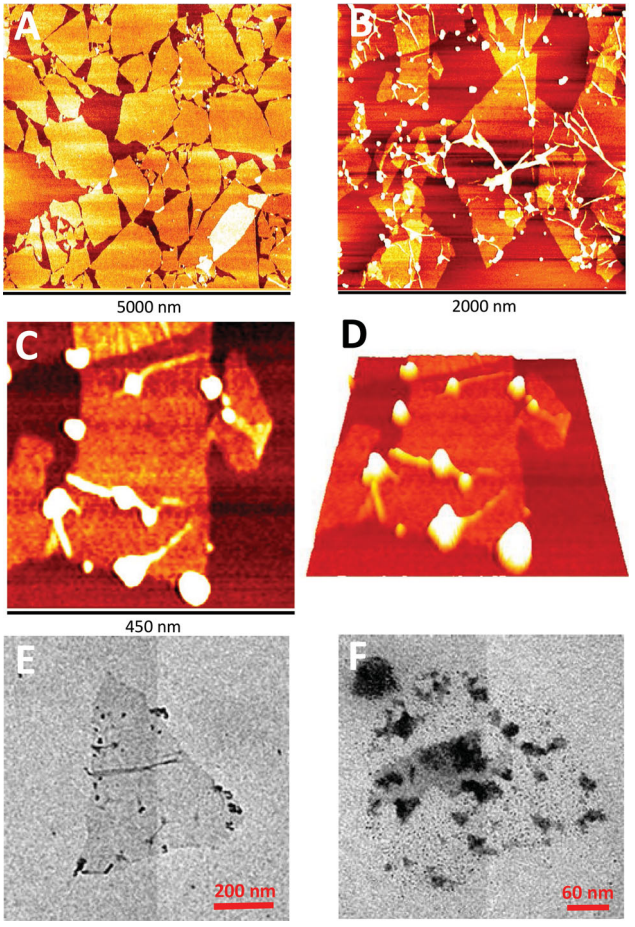

Figure 2. AFM and TEM images of various nanosheets. A) An AFM image of RGO nanosheets, B) an AFM image of PBNPs-RGO hybrid nanosheets with a larger scanned area, C,D) high-resolution topography (C) and three-dimensional (D) AFM images of PBNPs–RGO hybrid nanosheets, and E,F) TEM images of PBNPs–RGO hybrid nanosheets. The AFM substrate used is mica. The scanned areas: A) 5 μm × 5 μm, B) 2 μm × 2 μm, C) and D) 0.45 μm × 0.45 μm.

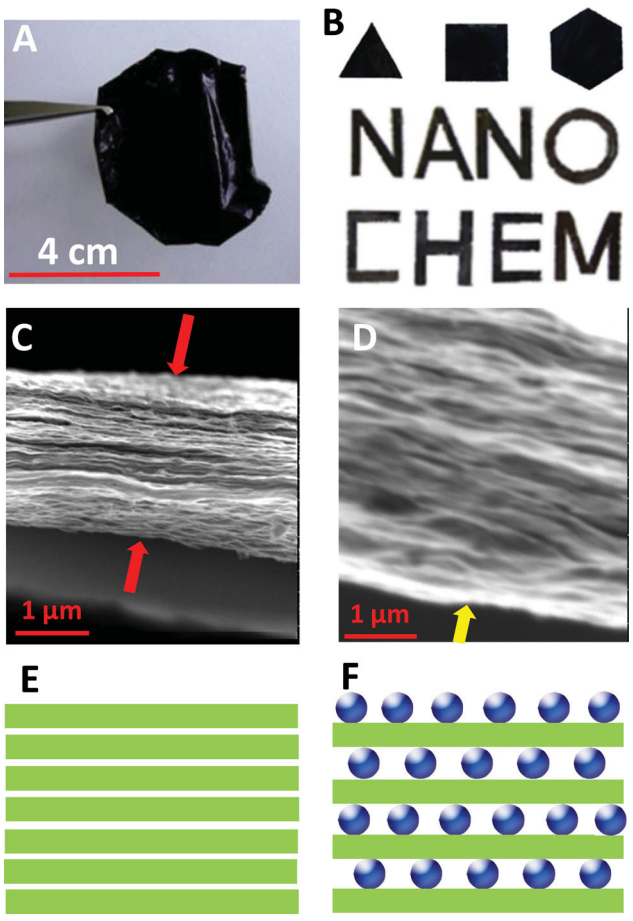

Figure 3. Photographs and SEM images of graphene papers. A,B) Photographs of different-shaped patterns and letters of PBNPs–RGO papers. Cross-sectional SEM images of C) RGO and D) PBNPs–RGO papers. Schematic illustrations of proposed side-view structures of E) RGO and F) PBNPs–RGO papers.

2.3. Physical Properties of PBNPs Doped Graphene Papers

PBNPs doped graphene papers were prepared by flow-directed assembly of PBNPs–RGO hybrid nanosheets via vacuum filtration (Scheme 1).[1] GO and RGO papers (i.e., without PBNPs) were prepared in the same way and used as reference systems. Prior to use, the papers were annealed at 220 °C for 2 h to enhance electrical conductivity. The resulting PBNPs–RGO papers are mechanically robust and can be cut into patterns of any shape. **Figure 3**A,B shows examples of various patterns. These include an irregular large piece (Figure 3A), triangular, rectangular and hexagonal small pieces (the top panel in Figure 3B) and various letters forming "NANO-CHEM" (the middle and bottom panels in Figure 3B). By controlling the amount of PBNPs–RGO hybrids, the papers with 1–20 μm thickness can be steadily prepared. Without peeling off the support porous membrane (as described in the Experimental Section, polycarbonate was used in the present work), the paper-like ultrathin graphene films with the thickness down to 100–200 nm can be also constructed with reasonable reproducibility.

The prepared papers were systematically characterized to disclose their chemical components, morphology, conductivity and other physical features. Fourier transform infrared (FTIR) spectra offer qualitative evidence for the presence of PBNPs in the graphene papers (Supporting Information, Figure S8). In contrast to RGO papers, the C–N stretching vibration at 2090 cm^{-1} and Fe–C–N–Fe stretching at 500 cm^{-1} from PB[46] are clearly observed in PBNPs–RGO papers. In addition, the O–H–O bending mode around 1600 cm^{-1} is also observed,[47] an indication of water molecules also trapped together with PBNPs in the graphene papers which could provide a microenvironment for accommodation of bio-macromolecules (see Section 2.5).

The surfaces of the papers are smooth, as shown by SEM (Supporting Information, Figure S9). The presence of PBNPs does not roughen the paper surfaces most likely due to the small size of PBNPs (around 6 nm), but does increase the spacing between the RGO layers as revealed by the cross-sectional SEM images (Figure 3C,D; Supporting Information,

Figure S10). Compared to RGO papers, the PBNPs–RGO papers appear to be "thicker" (compare the SEM images in Figure 3C,D), when the same RGO amount was used in the preparation of RGO and PBNPs–RGO papers. This is expected, because PBNPs were pre-adsorbed on the RGO nanosheets. As a result, PBNPs are intercalated between the RGO layers and uniformly distributed within the paper, as schematically illustrated by the structures proposed in Figure 3E,F.

Quantification of the layer spacing in graphene papers could be interesting and desired, but it needs high-resolution microscopic images which is hardly fulfilled by SEM. The SEM images shown in Figure 3C,D are cross-sectional images with the aim to visualize the layered structures and to qualitatively compare the apparent structural difference of two types of graphene papers (i.e., RGO and PBNPs–RGO papers) when the same RGO amount was used in the preparation of papers. The size of synthesized single layer RGO nanosheets and PBNPs is 0.8 nm in thickness and 6 nm in diameter, respectively. For example, the PBNPs–RGO paper with an overall thickness of 1 μm is thus estimated to contain approximately 140 hybrid layers, assuming that the hybrid nanolayers are closely packed.

Thermal gravity analysis (TGA) of GO, RGO and PBNPs–RGO papers was also performed. As shown in the Supporting Information (Figure S11), the observations for GO and RGO papers are similar to those in previous reports.[5–7] Briefly, a slight mass loss occurred below 200 °C similarly for all three types of sample, mainly due to evaporation of loosely adsorbed water. With increasing temperatures, a dramatic mass drop was detected around 200 °C for GO papers only, arising from decomposition of oxygen-containing functional groups. The mass loss at this temperature was also observed for RGO and PBNPs–RGO samples, but to a much lesser extent. These observations are, thus, consistent with the fact that most oxygen-containing functional groups were removed from GO by chemical reduction. Compared to RGO papers, there is an additional but slightly mass loss around 500 °C for PBNPs–RGO samples. This is attributed to the thermal removal of coordinated water in the PBNPs.

Electrical conductivity is of crucial importance for applications of graphene papers in electronic devices and electrochemistry. To gain an overview picture, we measured three types of resistance (or conductivity) with the results provided in the Supporting Information (Table S1). Pure PBNPs are poorly conductive as expected. For example, the surface resistance of PBNPs films was too large (>200 kΩ sq^{-1}) to be measured by the four-point probe mode. The incorporation of PBNPs into an RGO matrix results in a dramatic decrease in surface resistance down to 6.9 kΩ sq^{-1}, even if the nanocomposite still has a higher resistance than that for pure RGO papers. However, volume resistance and vertical conductivity of RGO and PBNPs–RGO papers are comparable (Supporting Information, Table S1). In terms of electrochemical applications, RGO in hybrid papers can, thus, serve not only as a current collector, but also a conductivity-enhancing matrix for PBNPs. Note that all these conductivity measurements were performed in air. However, electrochemical impedance spectroscopy (EIS) offers the feasibility to evaluate apparent ionic conduction of RGO and PBNPs–RGO papers in liquid environments under potential control, as described in the next section.

2.4. Electroactivity of PBNPs Confined in Graphene Papers

To facilitate electrochemical measurements, graphene papers were cut into rectangular pieces (e.g., 0. 5 cm × 3 cm) as free-standing working electrodes with an active area of 0.25 cm^2 (i.e., 0.5 cm × 0.5 cm). All electrochemical measurements were conducted with a three-electrode system and the potentials are referred to a saturated calomel electrode (SCE).

PBNPs confined in graphene papers remains highly electroactive. Cyclic voltammograms (CVs) shown in **Figure 4**A,B reveal that heterogeneous electron transfer (ET) reactions arising from confined PBNPs are reversible, with a pair of redox peaks at a formal redox potential of 0.18 V very close to that obtained for PBNPs in homogeneous solution (Supporting Information, Figure S4A) or in the immobilized state (Supporting Information, Figure S5). The relationship between the peak currents (I_p) and scan rate (υ) was evaluated by a series plots of I_p versus υ^x with x = 0.5–1.0 (Supporting Information, Figure S12). The best linear fit with a zero intercept is obtained for x = 0.7. This is an indication that the ET kinetics is controlled by mixed diffusion and surface confinement. Physical diffusion (or moving) of PBNPs within graphene papers is very unlikely, but strong electronic interactions between PBNPs could be expected due to the thin spacing (i.e., RGO nanosheets with atomic-layer thickness) that separates PBNPs (Figure 3F). Such electronic interactions could lead to diffusion-like controlled behavior in electrochemical ET. The rate constant estimated by the Laviron method[48,49] is about 5.2 s^{-1}. However, this value is at best a rough approximation and very likely underestimated due to complex rate-limiting steps (i.e., a mixture of diffusion and surface processes). An alternative explanation is that the redox transition of PB needs counter ions (cations) for charge compensation[50] and that difussion of cations (K^+ in the present case) from the electrolyte solution into graphene papers plays a significant role in determining the ET kinetics. This notion is particularly crucial when PB materials are confined in a nanoscale space, as pointed out by a recent report where PB was located inside carbon nanotubes.[40]

Electrochemical impedance spectra (EIS) were recorded under various experimental conditions. First, at fixed frequency, the apparent impedance of both RGO and PBNPs–RGO papers is potential-dependent and increases with potentials shifted positively (**Figure 5**A,B). Interestingly, in contrast to the conductivity measured in air (Supporting Information, Table S1), PBNPs–RGO papers appear to be more conductive than RGO papers in electrochemical environments. Besides, a sharp impedance decrease is observed around 0.18 V (i.e., the PBNP formal redox potential) for PBNPs–RGO papers (Figure 5B). Thus, the apparent conductance of PBNPs–RGO in liquid environments is also dependent on the redox states of the PBNPs, suggesting that PBNPs–RGO papers at the equilibrium PBNP redox state have a maximum ionic conductance. This characteristics could be a notable advantage for the use of PBNPs–RGO papers in electrocatalysis and electrochemical sensors, compared to their possible applications in solid-state devices.

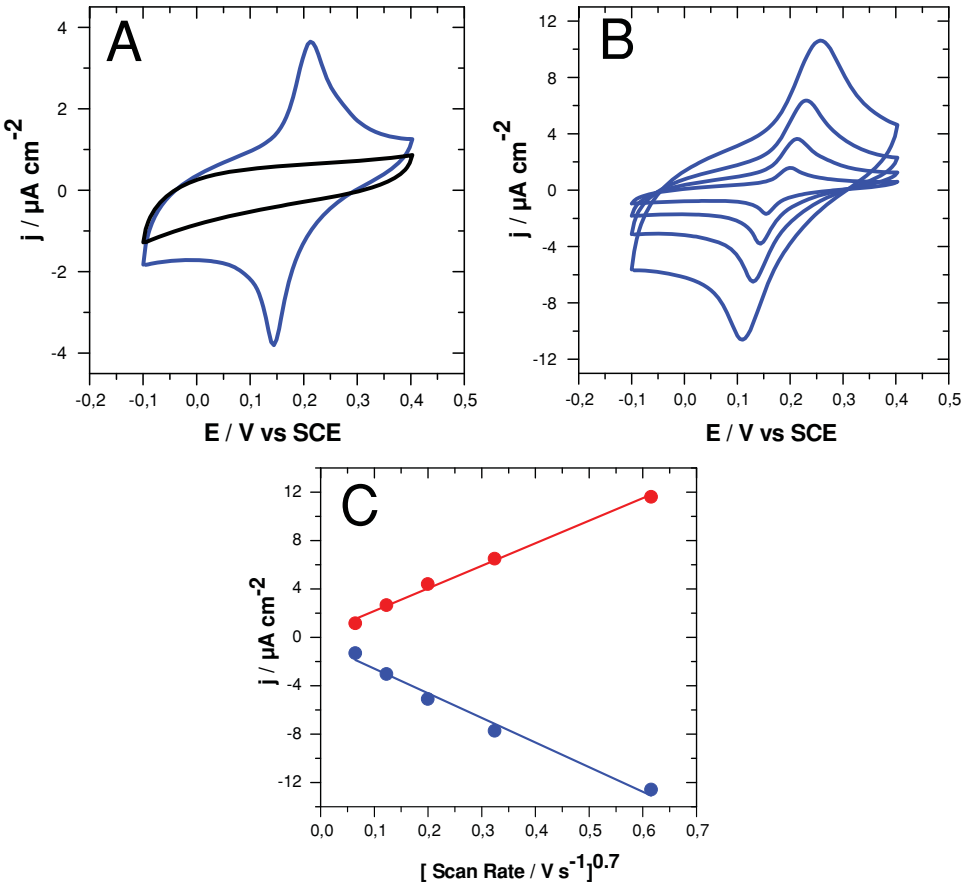

Figure 4. Voltammetric evaluations of electroactivity of PBNPs in graphene-PB hybrid papers. A) Comparison of cyclic voltammograms (CVs) of RGO alone (black curve) and PBNPs–RGO (blue curve) papers, scan rate 50 mV s^{-1}; B) CVs obtained at PBNPs–RGO papers with different scan rates of 20, 50, 100 and 200 mV s^{-1}; and C) the relation between the peak currents and scan rate. Electrolyte: 0.1 M phosphate buffer (pH 6.0) containing 0.1 M KCl used in all the measurements.

However, the intrinsic electrical conductivity of graphene papers was in fact not modulated by liquid environments, as indicated by the intercepts at *X*-axis in Figure 5C,D as approximately 4 and 8 KΩ for RGO and PBNPs–RGO papers, respectively. The oberved conductance enhancement should, thus, be attributed to electrochemical reactions of confined PBNPs.

The EIS spectra were then obtained at a fixed potential of 0.18 V for two types of papers, as compared in Figure 5C,D. While the EIS spectra for RGO papers are featureless (Figure 5C), the EIS spectra for PBNPs–RGO papers are characterized by a pseudo semicircle in the Nyquist plot (Figure 5D) with the ET resistance (R_{ct}) estimated as 4 kΩ. The experimental data were further fitted using an equivalent circuit, and the results are given in the Supporting Information (Figure S13). These observations are consistent with the voltammetric results (Figure 4A,B).

Finally, the EIS spectra were recorded in the presence of a redox probe consisting of $[Fe(CN)_6]^{3-}$ and $[Fe(CN)_6]^{4-}$ in electrolyte solutions. As expected, RGO papers favor the difussion-controlled $[Fe(CN)_6]^{3-/4-}$ ET reaction (i.e., fast ET kinetics) (Supporting Information, Figure S14), likely due to relatively high electrical conductivity. However, PBNPs–RGO papers can still be used as electrochemical working electrodes supporting external redox reaction.

2.5. Electrocatalysis and Enzyme Bioelectrocatalysis at Graphene Papers

As the electroactivity of PBNPs confined in RGO papers was well preserved (Section 2.4), we next examined their electrocatalytic activity towards reduction of hydrogen peroxide (H_2O_2). Electrocatalytic reduction of H_2O_2 started at 0.4 V (vs SCE) and tended to reach a maximum effect at potentials more negative than –0.1 V (**Figure 6**A; Supporting Information, Figure S15A). The electrocatalytic current increases with increasing H_2O_2 concentration (Supporting Information, Figure S15B). In contrast, the reference RGO paper system has little activity for electrochemical reduction of H_2O_2. Direct electroreduction could not be detected until –0.2 V and with much smaller current (Supporting Information, Figure S15A). The presence of PBNPs thus reduces the overpotetnial at least 600 mV, and enables sensitively detecting H_2O_2 at favorable potentials, for example, between 0.0 and –0.1 V. A linear relation between electrocatalytic current density (j_{cat}) and H_2O_2 concentration is observed in the range of 1–7 mM, with the detection limit down to about 5 µM (Figure 6B). These electrocatalytic properties have laid a solid basis for further incorporation of redox enzymes as biosensing devices, which

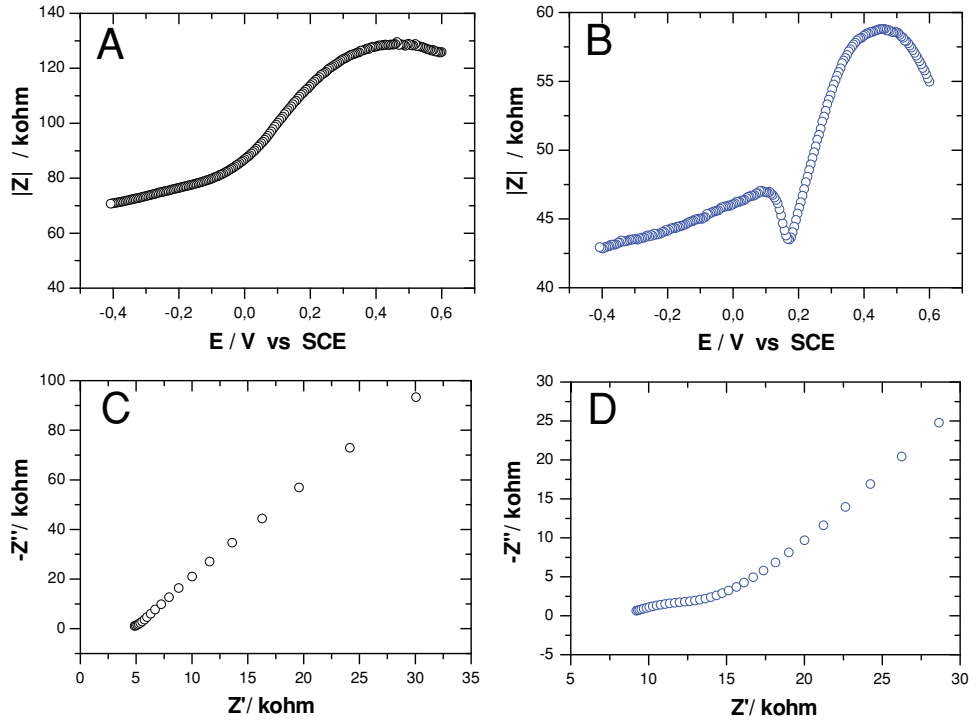

Figure 5. Electrochemical impedance spectra (EIS) of graphene papers. Comparison of the potential-dependent impedance spectra of A) RGO and B) PBNPs–RGO papers at a fixed frequency of 1 Hz; Nyquist plots of C) RGO and D) PBNPs–RGO papers at a fixed potential of 0.18 V (vs SCE, i.e., at the formal redox potential of PBNPs) with the frequency range of 10 000 to 0.5 Hz. Electrolyte was 0.1 M phosphate buffer (pH 6.0) containing 0.1 M KCl and an amplitude of 10 mV was used in all the measurements.

is addressed below with glucose oxidase (GOD) used as an example.

Pure RGO paper is structurally compact (Figure 3C) and largely hydrophobic, which makes it chemically incompatible for direct incorporation of bio-macromolecules such as proteins and enzymes. However, the layered integration of water-soluble PBNPs results in a much open structure (Figure 3D) with significantly enhanced hydrophilicity. This add-in structural and chemical feature is crucial for incorporation of enzyme into graphene papers. For example, incorporation of GOD in the present work was achieved either by soaking a piece of PBNPs–RGO paper in a GOD-containing buffer solution or by casting a few drops of GOD solution onto the PBNPs-RGO paper (details in the Experimental Section).

The addition of GOD in the papers increases the capacitive current response due to the more hydrophilic interfaces, but does not detectably affect the ET kinetics of PBNPs, as evaluated by cyclic voltammetry (Supporting Information, Figure S16A). The immobilized GOD retained its biocatalytic activity towards oxidation of glucose in the presence of dioxygen. The reduced GOD was re-oxidized by dioxygen, accompanied by generation of H_2O_2. The H_2O_2 generated was in turn electrocatalytically reduced by PBNPs in the paper and detected by the CVs (Supporting Information, Figure S16B). Such a redox catalytic cycle allows quantitatively analyzing glucose at favorable potentials (e.g., 0 or –0.05 V vs SCE) where signal interference from oxidation of ascorbic acid and/or uric acid can be avoided. Quantitative analysis was further carried out by recording the current versus time response curves upon successive injection of glucose, as shown in Figure 6C. The correlation between the electrocatalytic current and glucose concentration shows a linear relation up to about 6–8 mM (Figure 6D) with a sensitivity of 25 μA mM^{-1} cm^{-2} and the detection limit down to about 10 μM. It was found that the electrochemical analogue of the Michaelis-Menten equation for the relation between the electrocatalytic current density and the substrate concentration[51] applies and can be used to fit the experimental data. The apparent Michaelis-Menten constant (K_M) is estimated as 3.8 mM. This value is lower than those reported in most previous studies[52,53] but very close to a recently reported one (2.7 mM) where GOD was co-immobilized together with nickel oxide nanoparticles[54] on glassy carbon electrodes. A wide range of apparent K_M values (e.g., 5 to 60 mM) for this enzyme have been reported to date, mainly depending on the types of support matrix (e.g., metals, carbon electrodes and various polymers) and immobilization methods (e.g., covalent linking and non-convalent encapsulation).[52,53] Our results suggest that GOD confined in PBNPs–RGO papers shows a high binding affinity to substrate and, as such, its three-dimensional structures are well preserved.

It is noted that the detection limits of both H_2O_2 and glucose at PBNPs–RGO papers are relatively high, compared to these obtained at polymer–PB–GOD[55] or polymer–GOD–metllic NPs[56] systems. However, the present detection limit is still at the μM level. Since the blood sugar level is in the mM ranges (e.g., about 5.5 mM for the mean normal blood glucose level in humans), the GOD–PBNPs–RGO papers should hold potential

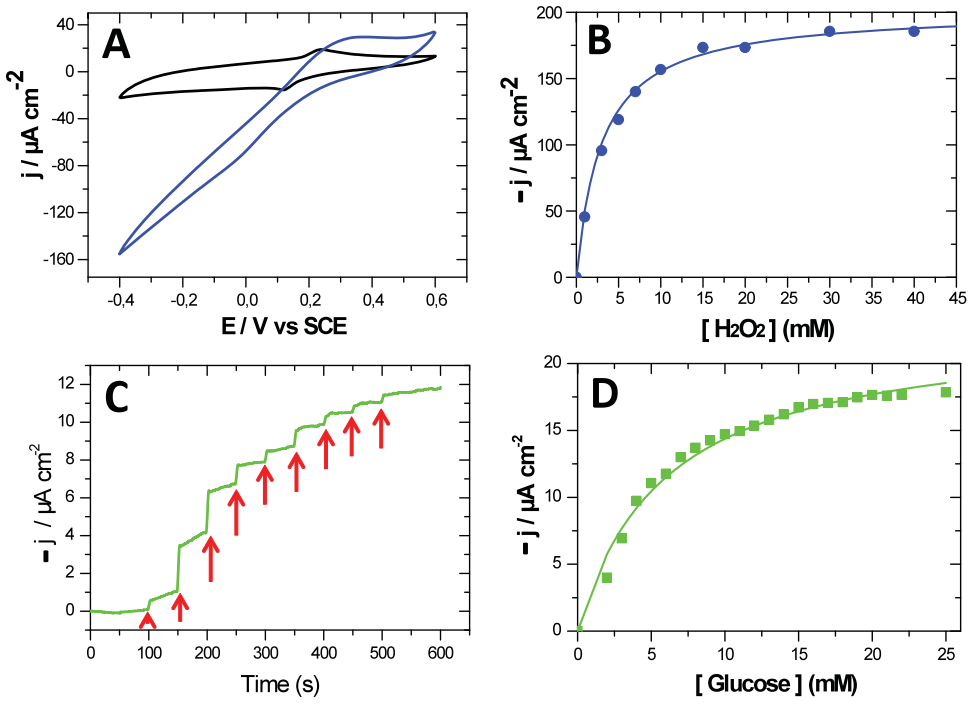

Figure 6. Electrocatalysis and biocatalysis. A) CVs of PBNPs–RGO paper electrodes in the absence (black curve) and presence (blue curve) of 10 mM H_2O_2; B) the dependence of electrocatalytic currents on concentrations of H_2O_2 in the range 0–40 mM at –0.1 V; C) the time course of responses of GOD–PBNPs–RGO papers to glucose at a fixed potential of –0.05 V (vs SCE) with 1 mM increment in injections; D) the dependence of electrocatalytic currents on concentrations of glucose in the range 0–25 mM. Electrolyte: 0.1 M phosphate buffer containing 0.1 M KCl (pH 6.0).Scan rate in (A): 20 mV s^{-1}.

as free-standing and disposable glucose sensors for applications in fast tests of blood sugar levels. Furthermore, the present work is largely focused on the preparation and characterization of PBNPs–RGO nanohybrids. To improve the sensitivity and detection limit, it is highly desired to further optimize fabrication of PBNPs–RGO nanohybrids based chemical sensors and biosensors in ongoing research.

3. Conclusions

Two types of highly stable, low-cost and chemically compatible nanoscale materials, RGO and Prussian blue nanoparticles, were synthesized and used as building blocks to prepare electrically enhanced and functionally endorsed nanohybrid electrocatalyst. Stable PBNPs–RGO hybrid sheets were formed via chemical interactions between two components. The present approach facilitates preparation of layered doping with electroactive PBNPs and free-standing graphene papers. PBNPs doped graphene papers show high-performance electrocatalysis towards reduction of hydrogen peroxide and can be used alone as flexible chemical sensors for potential applications in detection of hydrogen peroxide or/and other organic peroxides. PBNPs–RGO papers are further capable of biocompatible accommodation of enzymes for development of free-standing enzyme based biosensors, which is exemplified by glucose oxidase in the present work. On the basis of notable advantages of high stability, low cost and efficient electrocatalysis, this kind of nanohybrid materials has potential to be produced in a large scale and offers a broad range of possible applications as electron transfer mediators and nanoscale electrocatalysts, particularly in fabrication of flexible sensing devices as well as in electrocatalytic energy conversion.

4. Experimental Section

Chemicals and Materials: Graphite power (<20 µm, synthetic), potassium persulfate ($K_2S_2O_8$, ≥ 99%), phosphorus pentoxide (P_2O_5, ≥98%), potassium permanganate ($KMnO_4$, ≥99%), potassium phosphate dibasic (K_2HPO_4, ≥99.999%), hydrazine hydrate solution (50–60%), sulfuric acid (H_2SO_4, 95–97%), ammonia solution (25%), iron (III) nitrate nonahydrate $Fe(NO_3)_3$ (≥99.5%), and potassium chloride (KCl, ≥99%) were all from Sigma-Aldrich and used as received. Potassium hexacyanoferrate (III) ($K_3[Fe(CN)_6]$, 99%), potassium hexacyanoferrate (II) trihydrate ($K_4[Fe(CN)_6]\cdot 3H_2O$, ≥99%), potassium phosphate monobasic (KH_2PO_4, ≥99.5%), and hydrogen peroxide (H_2O_2, 30%) were obtained from Merck. Iron (III) chloride ($FeCl_3$, 98%) from Riedel-de Haën was used. Glucose oxidase (GOD, E. C.1.1.3.4) from *Aspergillus niger* (Type X-S, 100 000–250 000 U g^{-1}) and D-(+)-glucose (≥99.5%) were from Sigma-Aldrich. Milli-Q water (18.2 MΩ cm) was used throughout.

Synthesis of PBNPs, GO and RGO: PBNPs dispersions were synthesized by the reported method[41] with modifications.[42] The detailed procedure is described in the Supporting Information. Graphene oxide (GO) was prepared by the modified Hummer's method[45,57,58] with the details provided in the Supporting Information. RGO were obtained by chemical reduction of GO with hydrazine (5%), after addition of ammonia solution and refluxing the mixture under stirring for 2 h on a water bath at 95 °C.

Preparation of Freestanding GO, RGO and RGO–PBNP Papers: Graphene papers were fabricated by vacuum filtration of dispersions through a nuclepore polycarbonate membrane (ϕ 47 mm, 0.2 µm pores,

Whatman) using a stirred ultrafiltration cell (Millipore Corporation, USA). The thickness of GO and RGO papers was controlled by the amount of RGO dispersions. For example, most GO and RGO papers were made using the 1–5 mL stock solutions (0.2 mg mL^{-1}). PBNPs–RGO papers were fabricated by the same method but using PBNPs–RGO hybrid dispersions with a typical ratio of 1:8 (w/w, PBNPs:RGO). Prior to use, all graphene papers were subjected to annealing at 220 °C for 2 h. For electrochemical measurements, GO, RGO and RGO–PBNPs papers were cut into rectangular pieces (e.g., 0.5 cm × 3 cm) with an effective area of 0.5 cm × 0.5 cm.

Preparation of Enzyme Containing Graphene Papers: To incorporate enzyme into the papers, GO, RGO or PBNPs–RGO papers were soaked in glucose oxidase (GOD) solutions (2–5 mg mL^{-1} GOD) at 4 °C overnight. Before used in measurements, the graphene papers were rinsed with Milli-Q water and buffer solutions for at least three times, to remove loosely attached enzyme. Alternatively, GOD solution (e.g., 20 µL 5 mg mL^{-1}) was cast on graphene papers and then dried at 4 °C overnight. These two immobilization methods yielded similar results.

Instrumental Methods: UV-vis measurements were carried out using an Agilent Instrument Exchange Service Model G1103A. A 5500 AFM System (Agilent Technologies) was used for AFM imaging. All images were acquired in the tapping model. FTIR spectra were recorded by a PerkinElmer instrument (USA). The conductivity of RGO papers, PBNPs films and PBNPs–RGO papers were measured by a four-point probe setup (SZT-2A, Tongchuang Electronic Co., Ltd, China). TEM imaging was performed using a Tecnai G2 T20 from FEI Company (Oregon, USA) and SEM imaging by a Carl Zeiss EVO MA10 microscope. Thermogravimetric analysis (TGA, Netzsch STA 409PC) was carried out under an N_2 atmosphere, at a relatively slow heating rate of 5 °C min^{-1}.

Electrochemical measurements were carried out at room temperature (23 ± 2 °C) using an Autolab System (Eco Chemie, Netherlands) controlled by the general purpose electrochemical system software or/and using a CHI 760C electrochemical workstation. The three-electrode system was used throughout, consisting of a saturated calomel electrode (SCE) as reference electrode, a platinum coiled wire as counter electrode, and a piece of graphene paper as working electrode. The electrolyte used throughout was 0.1 M phosphate buffer (pH 6.0) containing 0.1 M KCl. Electrochemical impedance spectra (EIS) were recorded with an amplitude of 10 mV for various solutions without and with the $[Fe(CN)_6]^{3-/4-}$ redox probe.

Supporting Information

Supporting Information is available from the Wiley Online Library or from the author.

Acknowledgements

This work was supported by the Danish Research Council for Technology and Product Science (to Q.C., Project No. 12-127447), the Lundbeck Foundation (to Q.C., Grant No. R49-A5331) and the NanoScience Center at the University of Copenhagen. We thank the crucial help from Dr. Dirch H. Petersen at DTU Nanotech in some of conductivity measurements, Christian Enelbrekt for the TEM imaging, Xiaolong Zhu for the SEM experiments, and Dr. Qingfeng Li for access to the SEM facility. S.H. acknowledges a Hans C. Ørsted Postdoc Fellowship offered by the Technical University of Denmark. S.G. acknowledges the Universities Denmark for a visiting Ph.D studentship.

Received: February 16, 2013
Revised: March 27, 2013
Published online: May 10, 2013

[1] D. A. Dikin, S. Stankovich, E. J. Zimney, R. D. Piner, G. H. B. Dommett, G. Evmenenko, S. T. Nguyen, R. S. Ruoff, *Nature* **2007**, *448*, 457.
[2] S. Stankovich, D. A. Dikin, R. D. Piner, K. A. Kohlhaas, A. Kleinhammes, Y. Jia, Y. Wu, S. T. Nguyen, R. S. Ruoff, *Carbon* **2007**, *45*, 1558.
[3] S. Park, R. S. Ruoff, *Nat. Nanotechnol.* **2009**, *4*, 217.
[4] F. Yavari, N. Koratkar, *J. Phys. Chem. Lett.* **2012**, *3*, 1746.
[5] F. Xiao, Y. Q. Li, X. L. Zan, K. Liao, R. Xu, H. W. Duan, *Adv. Funct. Mater.* **2012**, *22*, 2487.
[6] H. C. Gao, Y. X. Wang, F. Xiao, C. B. Ching, H. W. Duan, *J. Phys. Chem. C* **2012**, *116*, 7719.
[7] F. Xiao, J. B. Song, H. C. Gao, X. L. Zan, R. Xu, H. W. Duan, *ACS Nano* **2012**, *6*, 100.
[8] J. Liang, Y. Huang, J. Oh, M. Kozlov, D. Sui, S. Fang, R. H. Baughman, Y. Ma, Y. Chen, *Adv. Funct. Mater.* **2011**, *21*, 3778.
[9] B. G. Choi, H. Park, T. J. Park, M. H. Yang, J. S. Kim, S.-Y. Jang, N. S. Heo, S. Y. Lee, J. Kong, W. H. Hong, *ACS Nano* **2010**, *4*, 2910.
[10] D. W. Wang, F. Li, W. Ren, Z. G. Chen, J. Tan, Z. S. Wu, I. Gentle, G. Q. Lu, H. M. Chen, *ACS Nano* **2009**, *3*, 1745.
[11] Y. Zhu, M. D. Stoller, W. Cai, A. Velamakanni, R. D. Piner, D. Chen, R. S. Ruoff, *ACS Nano* **2010**, *4*, 1227.
[12] A. Abouimrane, O. C. Compton, K. Amine, S. T. Naguyen, *J. Phys. Chem. C* **2010**, *114*, 12800.
[13] H. Gwon, H. S. Kim, K. U. Lee, D. H. Seo, Y. C. Park, Y. S. Lee, B. T. Ahn, K. Kang, *Energy Environ. Sci.* **2011**, *4*, 1277.
[14] G. Wang, K. Sun, F. Lu, H. Sun, M. Yu, W. Jiang, C. Liu, J. Lian, *Small* **2012**, *8*, 452.
[15] X. Wang, X. Cao, L. Bourgeois, H. Guan, S. Chen, Y. Zhong, D. M. Tang, H. Li, T. Zhai, L. Li, Y. Bando, D. Golberg, *Adv. Funct. Mater.* **2012**, *22*, 2682.
[16] F. Liu, S. Song, D. Xue, H. Zhang, *Adv. Mater.* **2012**, *24*, 1089.
[17] D. Wang, R. Kou, D. Choi, Z. Yang, Z. Nie, J. Li, L. V. Saraf, D. Hu, J. Zhang, G. L. Graff, J. Liu, M. A. Pope, I. A. Aksay, *ACS Nano* **2010**, *4*, 1587.
[18] Z. Li, Y. Mi, X. Lin, S. Lin, S. Yang, J. Wang, *J. Mater. Chem.* **2011**, *21*, 13991.
[19] S. Park, N. Mohanty, J. W. Suk, A. Nagaraja, J. An, R. D. Piner, W. Cai, D. R. Dreyer, V. Berry, R. S. Ruoff, *Adv. Mater.* **2010**, *22*, 1736.
[20] N. D. Luong, N. Pahimanolis, U. Hippi, J. T. Korhonen, J. Ruokolainen, L.-S. Johansson, J.-D. Nam, J. Seppala, *J. Mater. Chem.* **2011**, *21*, 13991.
[21] Y. J. Song, K. G. Qu, C. Zhao, J. S. Ren, X. G. Qu, *Adv. Mater.* **2010**, *22*, 2206.
[22] W. Hu, C. Peng, W. Luo, M. Lv, X. Li, D. Li, Q. Huang, C. Fan, *ACS Nano* **2010**, *4*, 4317.
[23] S. Some, S.-M. Ho, P. Dua, E. Hwang, Y. H. Shin, H. Yoo, J.-S. Kang, D.-K. Lee, H. Lee, *ACS Nano* **2012**, *6*, 7151.
[24] S. Park, K.-S. Lee, G. Bozoklu, W. Cai, S. T. Nguyen, R. S. Ruoff, *ACS Nano* **2008**, *2*, 572.
[25] H. Chen, M. B. Muller, K. J. Gilmore, G. G. Wallace, D. Li, *Adv. Mater.* **2008**, *20*, 3557.
[26] H. Bi, K. Yin, X. Xie, Y. Zhou, N. Wan, F. Xu, F. Banhart, L. Sun, R. S. Ruoff, *Adv. Mater.* **2012**, *24*, 5124.
[27] C. Valles, J. D. Nunez, A. M. Benito, W. K. Maser, *Carbon* **2012**, *50*, 835.
[28] S. Park, J. W. Suuk, J. An, J. Oh, S. Lee, W. Lee, J. R. Potts, J.-H. Byun, R. S. Ruoff, *Carbon* **2012**, *50*, 4573.
[29] A. R. Ranjbartoreh, B. Wang, X. Shen, G. Wang, *J. Appl. Phys.* **2011**, *109*, 014306.
[30] Y. Liu, B Xie, Z. Zhang, Q. Zheng, Z. Xu, *J. Mech. Phys. Solids* **2012**, *60*, 591.
[31] J. Xiang, L. T. Drzal, *ACS Appl. Mater. Interfaces* **2011**, *3*, 1325.
[32] Y. Tang, J. H. Gou, *Mater. Lett.* **2010**, *64*, 2513.

[33] Y. F. Li, Y. Z. Liu, W. Z. Shen, Y. G. Yang, M. Z. Wang, Y. F. Wen, *Appl. Phys. A Mater.* **2012**, *106*, 779.
[34] K. Itaya, I. Uchida, V. D. Neff, *Acc. Chem. Res.* **1986**, *19*, 162.
[35] Q. Chi, S. Dong, *Anal. Chim. Acta* **1995**, *310*, 429.
[36] A. A. Karyakin, O. V. Gitelmacher, E. E. Karyakina, *Anal. Chem.* **1995**, *67*, 2419.
[37] A. A. Karyakin, E. E. Karyakin, L. Gorton, *Anal. Chem.* **2000**, *72*, 1720.
[38] A. A. Karyakin, *Electroanalysis* **2001**, *13*, 813.
[39] F. Ricci, G. Palleschi, *Biosens. Bioelectron.* **2005**, *21*, 389.
[40] T. Wang, Y. Fu, L. Bu, C. Qin, Y. Meng, C. Chen, M. Ma, Q. Xie, S. Yao, *J. Phys. Chem. C.* **2012**, *116*, 20908.
[41] A. Gotoh, H. Uchida, M. Ishizaki, T. Satoh, S. Kaga, S. Okamoto, M. Ohta, M. Sakamoto, T. Kawamoto, H. Tanaka, M. Tokumoto, S. Hara, H. Shiozaki, M. Yamada, M. Miyake, M. Kurihara, *Nanotechnology* **2007**, *18*, 345609.
[42] H. Yan, M. Sc. thesis, Technical University of Denmark, DK-2800 Kongens Lyngby, Denmark, **2009**.
[43] J. Chen, Y. Miao, X. Wu, *Colloid J.* **2007**, *69*, 660.
[44] Y. Miao, J. Chen, X. Wu, K. Fang, A. Jia, J. Liu, *J. Nanosci. Nanotechnol.* **2007**, *7*, 2877.
[45] S. Y. Gan, L. J. Zhong, T. S. Wu, D. X. Han, J. D. Zhang, J. Ulstrup, Q. Chi, L. Niu, *Adv. Mater.* **2012**, *24*, 3958.
[46] E. Jin, X. F. Lu, L. L. Cui, D. M. Chao, C. Wang, *Electrochim. Acta* **2010**, *55*, 7230.
[47] C. Wang, L. Zhang, Z. H. Guo, J. G. Xu, H. Y. Wang, H. W. Shi, K. F. Zhai, X. Zhuo, *Electroanalysis* **2010**, *22*, 1867.
[48] E. Laviron, *J. Electroanal. Chem.* **1979**, *101*, 19.
[49] P. S. Jensen, Q. Chi, F. B. Grumsen, J. M. Abad, A. Horsewell, D. J. Schiffrin, J. Ulstrup, *J. Phys. Chem. C* **2007**, *111*, 6124.
[50] K. Itaya, H. Akahoshi, S. Toshima, *J. Am. Chem. Soc.* **1982**, *104*, 4767.
[51] Q. Chi, J. Zhang, P. S. Jensen, H. E. M. Christensen, J. Ulstrup, *Faraday Discuss.* **2006**, *131*, 181.
[52] C. G. J. Koopal, R. J. M. Notle, *Bioelectrochem. Bioenerg.* **1994**, *33*, 45.
[53] D. W. Kimmel, G. LeBlanc, M. E. Meschievltz, D. E. Cliffel, *Anal. Chem.* **2012**, *84*, 685.
[54] A. Salimi, E. Sharifi, A. Noorbakhsh, S. Soltanian, *Biosens. Bioelectron.* **2007**, *22*, 3146.
[55] C. Chen, Y. Fu, C. Xiang, Q. Xie, Q. Zhang, Y. Su, L. Wang, S. Yao, *Biosens. Bioelectron.* **2009**, *24*, 2726.
[56] Y. Fu, P. Li, Q. Xie, X. Xu, L. Lei, C. Chen, C. Zou, W. Deng, S. Yao, *Adv. Funct. Mater.* **2009**, *19*, 1784.
[57] W. S. Hummers, R. E. Offeman, *J. Am. Chem. Soc.* **1958**, *80*, 1339.
[58] N. I. Kovtyukhova, P. J. Ollivier, B. R. Martin, T. E. Mallouk, S. A. Chizhik, E. V. Buzaneva, A. D. Gorchinskiy, *Chem. Mater.* **1999**, *11*, 771.